

A FIRST-APM-SDSS survey for high-redshift radio QSOs

R. Carballo,¹ ^{*}, J.I. González-Serrano,² F.M. Montenegro-Montes,³ C.R. Benn,⁴
K.-H. Mack,³ M. Pedani,⁵ M. Vigotti³

¹ *Dpto. de Matemática Aplicada y Ciencias de la Computación, Univ. de Cantabria*

ETS Ingenieros de Caminos, Canales y Puertos, Avda de los Castros s/n, E-39005 Santander, Spain

² *Instituto de Física de Cantabria (CSIC-Universidad de Cantabria), Avda de los Castros s/n, E-39005 Santander, Spain*

³ *Istituto di Radioastronomia, INAF, via Gobetti 101, I-40129 Bologna, Italy*

⁴ *Isaac Newton Group, Apartado 321, E-38700 Santa Cruz de La Palma, Spain*

⁵ *Centro Galileo Galilei, E-38700 Santa Cruz de La Palma, Spain*

11 November 2018

ABSTRACT

We selected from the VLA FIRST survey a sample of 94 objects with starlike counterparts in the Sloan Digital Sky Survey, and with APM POSS-I colour $O - E \geq 2$, i.e. consistent with their being high-redshift quasars. 78 of the 94 candidates can be classified spectroscopically on the basis of either published data (mainly SDSS) or the observations presented here. The fractions of QSOs (51 out of 78) and redshift $z > 3$ QSOs (23 out of 78, 29 per cent) are comparable to those found in other photometric searches for high-redshift QSOs. We confirm that selecting colour $O - E \geq 2$ ensures inclusion of all QSOs with $3.7 \leq z \leq 4.4$. The fraction of $2 \leq z \leq 4.4$ QSOs with broad absorption lines (BALs) is 27 ± 10 per cent (7/26) and the estimated BAL fraction for radio loud QSOs is at least as high as for optically selected QSOs (~ 13 per cent). Both the high BAL fraction and the high fraction of LoBALs among BALs (four to five out of 7) in our sample, compared to previous work, are likely due to the red colour selection $O - E \geq 2$. The space density of radio loud QSOs in the range $3.7 \leq z \leq 4.4$ ($\bar{z} = 4.0$) with $M_{\text{AB}}(1450) \leq -26.6$ and $P \geq 10^{25.7} \text{ W Hz}^{-1}$ is $1.7 \pm 0.6 \text{ Gpc}^{-3}$. Adopting a radio-loud fraction of 13.4 ± 3 per cent, this corresponds to $\rho = 12.5 \pm 5.6 \text{ Gpc}^{-3}$, in substantial agreement with the cumulative luminosity function of SDSS QSOs in Fan et al. (2001a). We note the unusual flat-spectrum radio-luminous QSO FIRST 1413+4505 ($z = 3.11$), which shows strong associated Ly α absorption (rest-frame equivalent width $\sim 40 \text{ \AA}$) and an extreme observed luminosity, $L \sim 2 \times 10^{15} L_{\odot}$.

Key words: surveys – quasars: general – galaxies: high redshift – early Universe – radio continuum: galaxies

1 INTRODUCTION

This is the third of a series of papers presenting new samples of high-redshift radio QSOs selected by matching the FIRST catalogue of radio sources (Faint Images of the Radio Sky at Twenty-cm; Becker, White & Helfand 1995, White et al. 1997) with red starlike objects from the APM (Automated Plate Measuring Facility) catalogue of the POSS-I survey (McMahon & Irwin 1992).

Papers I and II (Benn et al. 2002, Holt et al. 2004) reported a sample of 18 $z > 3.6$ QSOs including the largest sample of $z > 4$ radio-selected QSOs then known. The search was carried out within a $\sim 7030 \text{ deg}^2$ region using the con-

straints: i) $E < 18.8$ and starlike, ii) $S_{1.4 \text{ GHz}} \geq 1 \text{ mJy}$, and iii) colour selection $O - E \geq 3$. This colour range includes an estimated 95 ± 1.5 per cent of $E < 18.8$ QSOs with redshift $3.8 < z < 4.5$ (Vigotti et al. 2003). On the basis of the 13 QSOs with $z \simeq 3.8 - 4.5$ and comparing to an equivalent sample at $z \simeq 2$ drawn from the FIRST Bright Quasar Survey of the north Galactic cap (FBQS-2, White et al. 2000), we showed (Vigotti et al. 2003) that the decline in space density of $M_{\text{AB}}(1450 \text{ \AA}) \leq -26.9$ QSOs ($H_0 = 50 \text{ km s}^{-1} \text{ Mpc}^{-1}$, $\Omega_M = 1$ and $\Omega_{\Lambda} = 0$ here and throughout the paper) was approximately a factor 2 between $z \sim 2$ and $z \sim 4$, significantly smaller than the value ~ 10 found for samples including lower luminosity objects (Fan et al. 2001a).

The Sloan Digital Sky Survey Data Release 3 (SDSS, Stoughton et al. 2002; DR3 Abazajian et al. 2005) provides

* E-mail: carballor@unican.es

Table 1. Right ascension and declination ranges of the four areas of sky included in the survey.

RA (h)	DEC (deg)
7.933 → 8.667	+30 → +46
8.733 → 9.600	+38 → +55
9.667 → 15.667	+42 → +58
15.733 → 16.667	+30 → +45

moderately deep CCD imaging in five bands *ugriz* covering $\sim 5282 \text{ deg}^2$. We present and discuss a new sample of high-redshift radio-selected QSO candidates in a 1378.5 deg^2 area of overlap between FIRST and SDSS DR3 in the north Galactic cap. The selection criteria are: i) $E \leq 19.1$ and starlike in APM, ii) $S_{1.4 \text{ GHz}} \geq 1 \text{ mJy}$, iii) radio-optical separation less than 1.5 arcsec , iv) colour $O - E \geq 2$ (including O non-detections) and v) starlike in SDSS. This new sample, with a wider colour range, has several advantages. Firstly, the SDSS photometric catalogue provides reliable morphological classification of the sources, allowing us to readily eliminate the galaxies classed as starlike in APM POSS-I. Secondly, SDSS provides $\sim 3 \text{ \AA}$ -resolution spectra and spectroscopic classifications of many objects, particularly those selected as QSO candidates on the basis of their *ugriz* colours, or as counterparts of FIRST sources. We continue to use the APM catalogue for colour selection since our previous work showed a high efficiency and completeness in the selection of $z > 3.85$ QSOs using $O - E \geq 3$ and with the new limit $O - E \geq 2$ we can check that no $z > 3.7$ QSOs have $O - E < 3$.

The paper is structured as follows. In Section 2 we present the sample and the status of the spectroscopic classification. Section 3 reports optical spectroscopy of part of the sample. The spectroscopic classification of the sample as QSOs, narrow emission line galaxies or stars is presented in Section 4.1. The distribution of optical magnitudes and $O - E$ colours is discussed in Section 4.2. In Section 4.3 the sample is compared with previous radio-selected QSO samples from the literature, in terms of the selection criteria and the resulting QSO redshift distribution. In Section 4.4 we comment briefly on the spectra of seven QSOs exhibiting strong blueshifted broad absorption lines (BALs) and we analyse the fraction of BAL QSOs in the sample. Section 4.5 is devoted to the peculiar QSO FIRST 1413+4505. In Section 4.6 we compute the absolute magnitudes, k -corrections and radio luminosities of the 10 QSOs with $z \geq 3.7$, and we discuss the completeness of a sub-sample of seven of them. In Section 5 we use this sample to calculate the space density of QSOs. Section 6 summarizes our conclusions.

2 SELECTION OF THE SAMPLE

The sample was selected from the 1378.5-deg^2 area defined in Table 1. This area includes most of the region covered by SDSS DR3 in the north Galactic cap, which is also covered by the FIRST survey and by the APM catalogue of POSS-I. The FIRST survey includes 122463 sources in this area with $S_{1.4 \text{ GHz}}$ (peak) $\geq 1 \text{ mJy}$, of which 113 have APM $E < 19.1$, $O - E > 2.0$ and lie within 1.5 arcsec of starlike objects in SDSS DR3. Eighteen of these were undetected in

APM POSS-I O but were detected in APS POSS-I O and had $\text{APS}(O - E) < 2$, and were therefore removed from the sample. For the source FIRST 1340+5619 we found a large difference between the SDSS and APM magnitudes ($r = 23.51$ versus $E = 18.99$) and the source was eliminated from the sample after confirming with SDSS that the APM counterpart is a blend. The final sample thus includes 94 candidate high-redshift radio QSOs.

Of these 94 candidates, spectra were first obtained for seven in papers I and II, for six in the literature (found using the NASA Extragalactic Database - NED) and for 41 by SDSS DR3 (which also reobserved nine of the thirteen previously discovered). In Section 3 we present TNG optical spectroscopy of 13 (randomly selected) of the 40 remaining candidates, and we classify an SDSS DR3 source given spectral class ‘unknown’ in the Sloan survey. Subsequent to these observations, SDSS DR4 (2005 June 30) reported spectroscopy of 10 of the remaining 27 candidates (and also of four of those observed here). In total, 78 of the 94 candidates (83 per cent) are now spectroscopically classified (see Section 4.1).

3 TNG OPTICAL SPECTROSCOPY

Spectra of 11 candidates (indicated in column 9 of Table 2) were obtained with the Telescopio Nazionale Galileo (TNG) on 2005 March 10 and 11 using the DOLORES (Device Optimized for LOW REsolution) spectrograph in long-slit mode. The LR-B grism was used, yielding a wavelength range $3000 - 8800 \text{ \AA}$ and dispersion $2.9 \text{ \AA pixel}^{-1}$. The detector was a thinned, back-illuminated Loral CCD with $15 \mu\text{m}$ pixels. Exposure times were typically 900 s. Three spectrophotometric standard stars were observed in order to calibrate the instrumental spectral response. The seeing was $\approx 1.8 \text{ arcsec}$, and the width of the slit was set to 2 arcsec , yielding a spectral resolution of 23 \AA , as measured from sky lines.

Standard data reduction was carried out using the IRAF[†] package. Arc-lamp exposures were used for the wavelength calibration, and yielded solutions with rms residuals $< 1.5 \text{ \AA}$. Small spectrum-to-spectrum wavelength shifts were corrected using sky lines in the science spectra. In most of the spectra, the two or three brightest sky emission lines were not completely removed in the sky subtraction. This did not affect spectral classification or redshift measurement, but for presentation in Figs. 1, 2 we manually cleaned some of the strongest residuals.

Spectra of two more candidates (FIRST 1343+4305 and FIRST 1405+5155) were obtained with similar instrumental set-up on the nights of 2005 July 12 and 13. Two spectra per object were taken, shifting the object along the slit to minimize the effect of detector artefacts and remove the OH sky lines. For each object, one 2D spectrum was subtracted from the other, to remove the background, then wavelength calibrated, aligned in the spatial direction and coadded. Ex-

[†] IRAF is distributed by the National Optical Astronomy Observatories, which is operated by Association of Universities for Research in Astronomy, Inc., under cooperative agreement with the National Science Foundation.

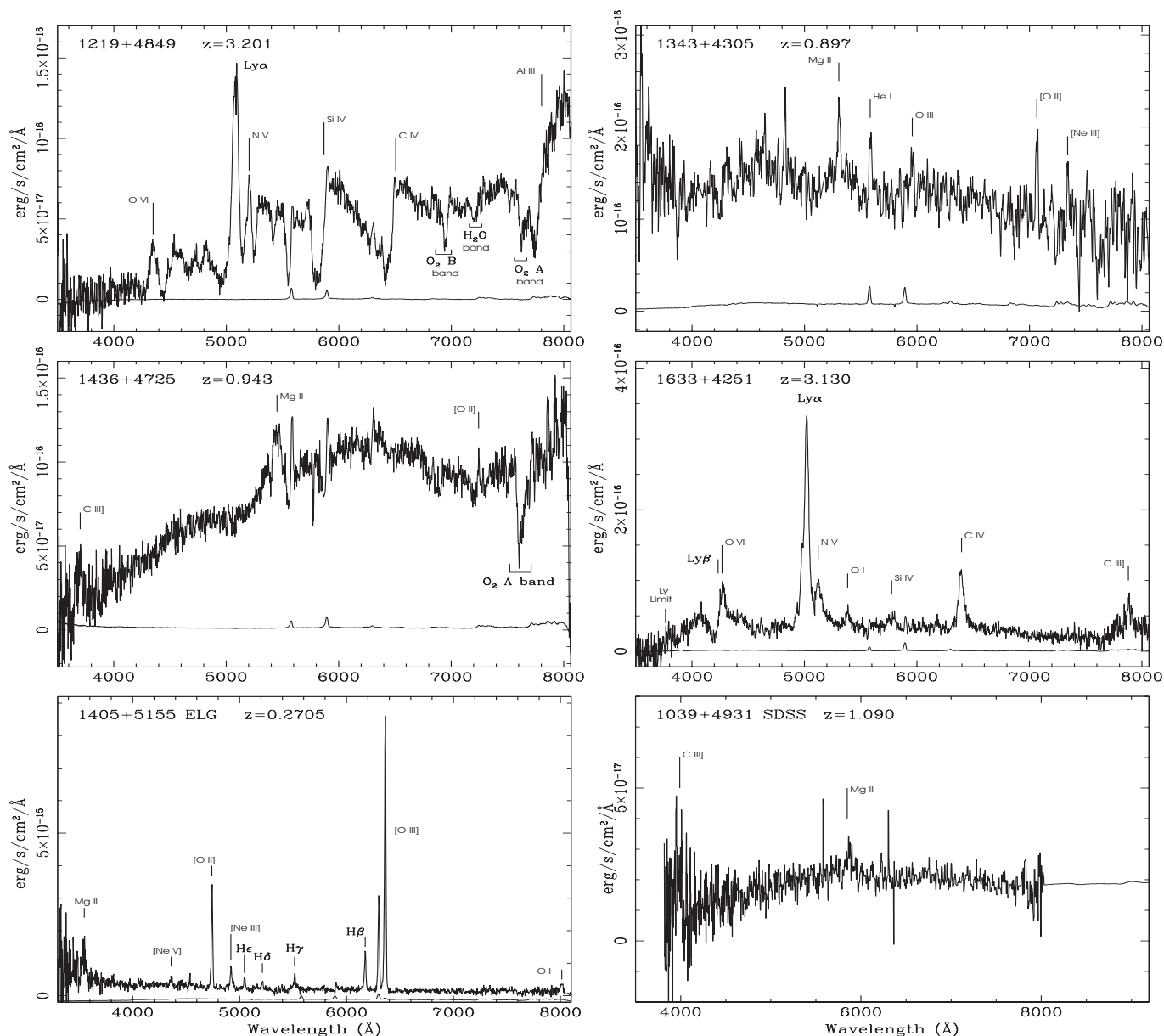


Figure 1. TNG spectra of the four QSOs and the emission-line galaxy identified for the first time here, and the SDSS spectrum of source FIRST 1039+4931, which was classified ‘unknown’ in SDSS. The night sky spectrum (scaled) is shown near the zero level in the TNG spectra. The emission features are labelled by ion (wavelengths from Vanden Berk et al. 2001).

posure times were 2×1800 s for 1343+4305 and 2×1200 s for 1405+5155.

The 13 objects include eight QSOs, one $z = 0.2705$ emission line galaxy (ELG), and four late-type stars. The redshift of each QSO was estimated as the average of the values measured from individual emission-line centroids (excluding Ly α , which is often affected by Ly α forest absorption). Six of the QSOs have $3.1 < z < 3.9$, the other two have $z = 0.897$ and $z = 0.943$.

The TNG spectra of the eight QSOs and the ELG are shown in Figs. 1 and 2. Fig. 1 also shows the SDSS DR3 spectrum of FIRST 1039+4931, classified ‘unknown’ in SDSS, but which we identify as a QSO at $z = 1.09$. Four of the eight QSOs were also observed in SDSS DR4, published af-

ter our TNG observations took place. The TNG spectra of these four objects are shown in Fig. 2.

4 PROPERTIES OF THE SAMPLE

4.1 Spectroscopic classification

Table 2 lists the basic optical and radio properties of the 94 objects in the sample, together with the spectroscopic classification and redshift, mostly from SDSS DR3 and DR4. The spectra were classified as one of: QSO (broad emission lines), emission-line galaxy (narrow emission lines), late-type star or early-type star. The sample of 94 objects includes 51 QSOs ($0.27 < z < 4.31$), 25 stars, two ELGs ($z = 0.27, 0.31$) and 16 objects with no optical spectrum, i.e. 78 out of 94 (83

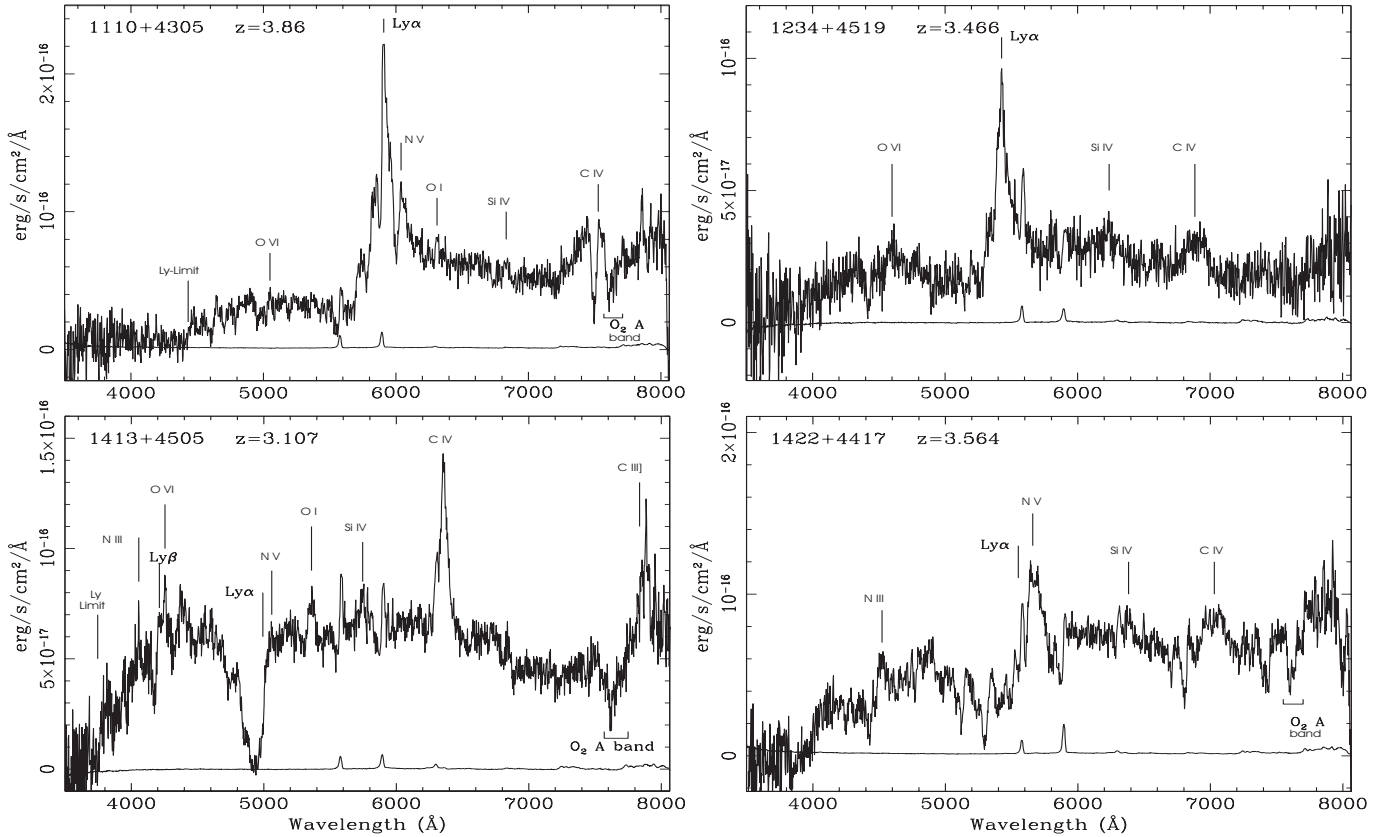


Figure 2. Spectra of four QSOs identified at the TNG and also observed by SDSS DR4.

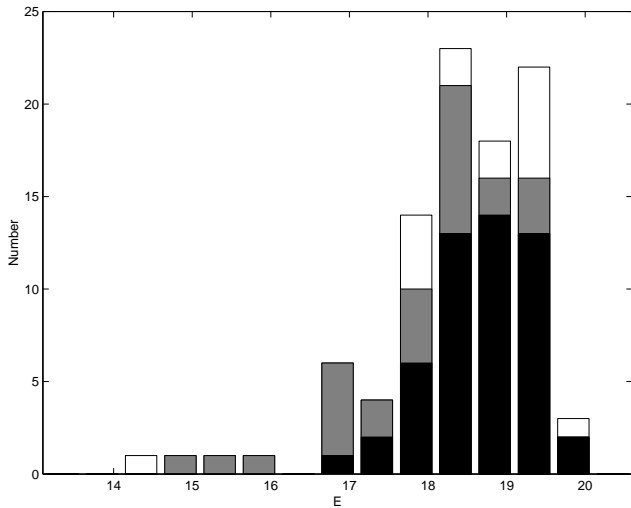


Figure 3. Distribution of corrected E magnitude. QSO identifications are shown in black, stars and ELGs in grey and unclassified sources in white.

per cent) are classified. Of the 78 objects with spectra, 38 per cent (30/78) are QSOs with $z \geq 2$, 29 per cent (23/78) are QSOs with $z \geq 3$ and 13 per cent (10/78) are QSOs with $z \geq 3.7$, confirming the efficiency of the adopted selection criteria for identifying moderate- to high- z QSOs. The efficiencies of previous radio QSO surveys are compared in Section 4.3.

4.2 Distribution of optical magnitudes and $O - E$ colours

In Table 2 and hereafter, unless otherwise indicated, the quoted POSS-I APM magnitudes are recalibrated with respect to APS (McMahon et al. 2002), and are corrected for Galactic reddening. This results in some of the sample having final $O - E < 2$ and $E > 19.1$ (the recalibrated E magnitudes are typically 0.3 ± 0.3 mags fainter than the original APM values). The histogram of the E magnitudes is shown in Fig. 3.

Fig. 4 shows the distribution $O - E$ versus E . QSOs have a broader $O - E$ colour range than stars. The ratio QSOs/stars increases from 21/12 in the range $17.1 < E \leq 18.6$ to 29/5 for $E > 18.6$ (see also Fig. 3). Assuming that the unclassified sources in Fig. 4 are either QSOs or stars, the distribution in $O - E$ versus E suggests that ~ 60 per cent are QSOs.

Fig. 5 (see also Fig. 6b) shows that the QSO colours redden significantly with redshift: the four measured values of $O - E$ and three out of six lower limits imply $O - E > 3$ for $z > 3.7$. This is due to the drop in intensity in the O band as it becomes more dominated by the region blueward of the Lyman limit, and the increase in intensity in the E band as $\text{Ly}\alpha$ enters the band.

An important conclusion from Fig. 5 is that the colour cut $O - E \geq 2$ includes most of the QSOs with $3.7 \leq z < 4.4$, and this result is in agreement with previous studies. In Vigotti et al. (2003) we estimated a fraction of $z > 3.8$ QSOs with $\text{APM}(O - E) > 3$ of 95 ± 1.5 per cent, using a sample

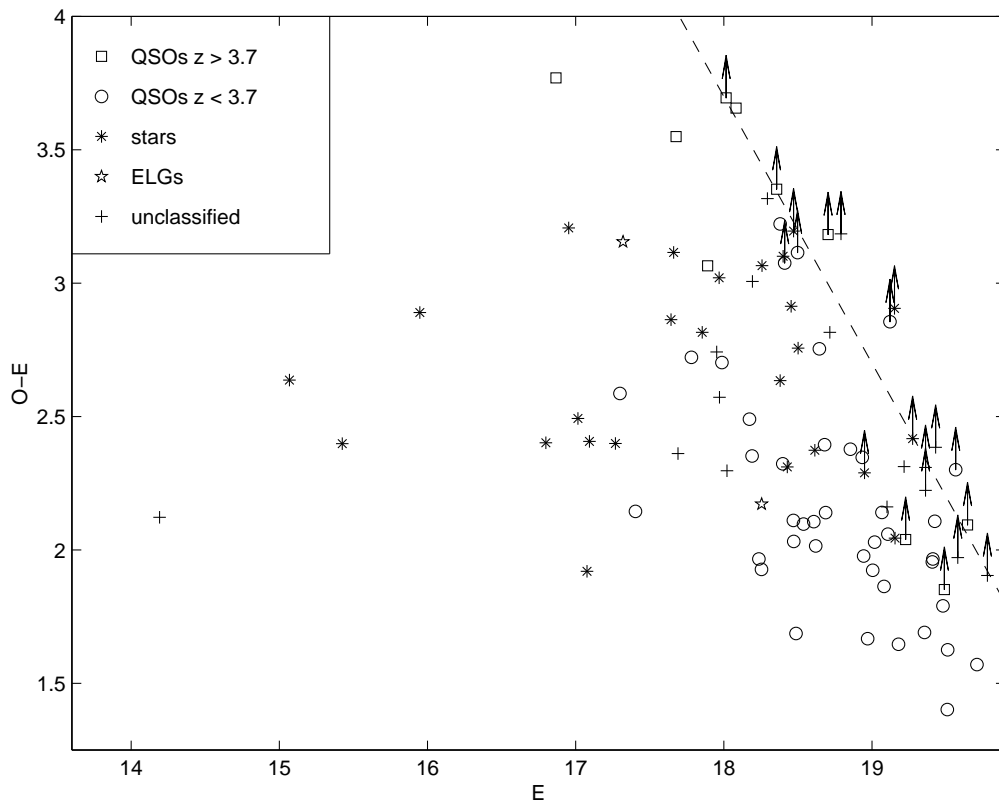


Figure 4. Colour-magnitude diagram for all 94 candidates in the sample. The dashed line corresponds to an assumed POSS-I blue plate limit $O = 21.7$ (referred to the APS calibration). Arrows show objects not detected in O band.

Table 3. Selection criteria and QSO fractions for FBQS-2 and for the current sample

	FBQS-2	This work
Area (deg ²)	2682	1378.5
E	≤ 17.8	$\leq 19.1^{(1)}$
$O - E$	≤ 2	$\geq 2^{(1)}$
Radio-opt separation (arcsec)	≤ 1.2	≤ 1.5
Starlike morphology	E or O	E and SDSS
Number of candidates	1238	94
Number of spec. class.	1130	78
Number of QSOs	636	51
Number of QSOs $2 \leq z < 3$	53	7
Number of QSOs $3 \leq z < 3.7$	12	13
Number of QSOs $z \geq 3.7$	0	10

1: O and E magnitudes as taken directly from APM

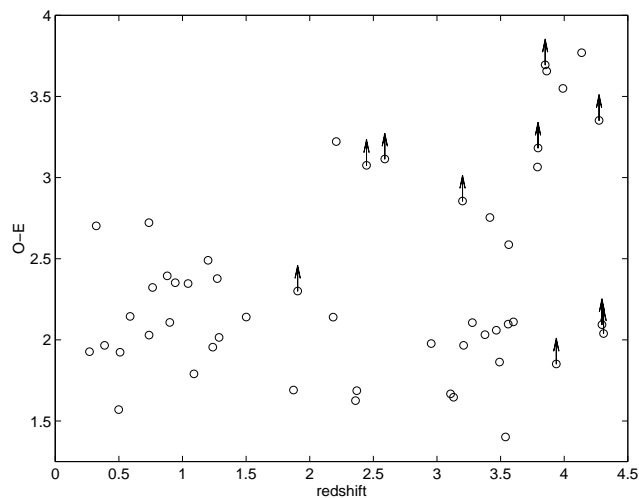


Figure 5. $O - E$ versus redshift for the QSOs in the sample.

with $E(\text{APM}) \leq 18.8$. In FBQS-2 (White et al. 2000, $O - E \leq 2$ and $E \leq 17.8$) 90 per cent of the QSO candidates were spectroscopically classified, and these included 636 QSOs, none of which had $z > 3.5$, although 12 had $3 < z < 3.5$. We are therefore confident that the number of QSOs we find with $3.7 \leq z \leq 4.4$ is limited only by the radio and E band flux density limits, with no QSOs missed due to the colour selection.

4.3 Comparison with other radio samples

The survey reported here can be considered complementary to FBQS-2. Both surveys select FIRST radio sources with starlike optical counterparts, but the colour criteria are $O - E \leq 2$ for FBQS-2 (blue-excess objects) and $O - E \geq 2$ for our work. In FBQS-2 objects were selected with $O - E \leq 2$ to eliminate galaxies, since catalogues based on photographic plates provide poor discrimination between stellar and non-stellar objects. The survey selection criteria, and the QSO

Table 4. Well-defined samples of $z \geq 3$ radio-selected QSOs

Reference, radio/opt limits (1)	Area (deg ²) (2)	Cands. (3)	Spec. Class. (4)	$z > 3.0$ (5)	$z > 3.7$ (6)
Hook et al. 1998 Green Bank $S_{5 \text{ GHz}} \geq 25$ mJy FIRST $S_{1.4 \text{ GHz}} \alpha_{1.4}^5 \geq -0.5$ APM POSS-I $E \leq 19.5$, $O - E \geq 1.2$	1600	73	50	6/50 12%	0/50 0%
Snellen et al. 2001 Green Bank $S_{5 \text{ GHz}} \geq 30$ mJy NVSS $S_{1.4 \text{ GHz}} \alpha_{1.4}^5 \geq -0.35$ APM $E < 19$, $O - E > 2$	6400	27	27	9/27 33%	5/27 19%
Hook et al. 2002 Green Bank $S_{5 \text{ GHz}} \geq 50$ mJy NVSS $S_{1.4 \text{ GHz}} \alpha_{1.4}^5 \geq -0.5$ APM UKST $R < 21$; $B - R \geq 1.5$ or $R - I \geq 1$ or $B - I \geq 2$	7265 <i>BR</i> (3637 <i>BRI</i>)	228	202	18/202 9%	12/202 6%
Holt et al. 2004 FIRST $S_{1.4 \text{ GHz}} \geq 1$ mJy APM $E < 18.8$, $O - E > 3$	7030	194	121	15/121 12%	15/121 12%
This work FIRST $S_{1.4 \text{ GHz}} \geq 1$ mJy APM $E \leq 19.1$, $O - E \geq 2$	1380	94	78	23/78 29%	10/78 13%

Col. (1): reference, optical and radio catalogues, and optical and radio flux-density and spectral-index ($S_\nu \propto \nu^\alpha$) limits.
(2): survey area. (3,4,5,6): number of candidates, number of candidates with spectroscopic classification and the fraction of the latter at redshifts $z > 3$ and $z > 3.7$.

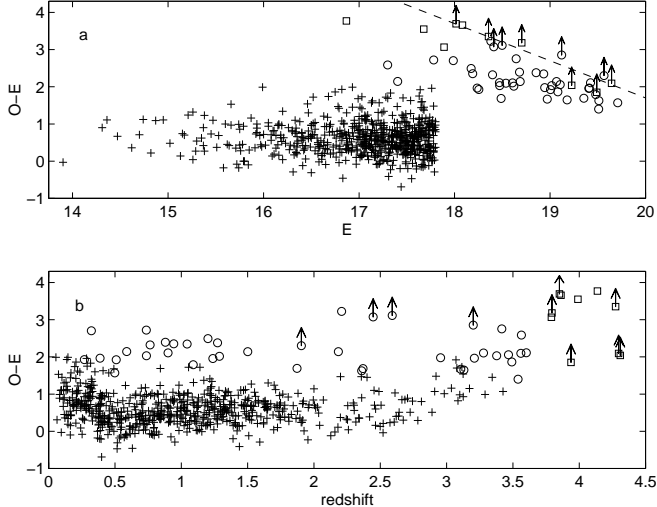


Figure 6. (a) $O - E$ versus E for the QSOs in FBQS-2 (crosses) and in this work (circles for $z < 3.7$, squares for $z \geq 3.7$). The dashed line corresponds to the assumed POSS-I blue plate limit $O = 21.7$. (b) $O - E$ versus z for the same QSOs.

fractions as a function of redshift, are compared in Table 3. Figs. 6a and 6b show $O - E$ versus E and $O - E$ versus z for the QSOs in the two surveys. Whereas the redshifts covered by FBQS-2 range up to 3.4, our sample includes redshifts up to 4.3 (Fig. 6b, Table 3), and this is a consequence of both the colour cut and the fainter magnitudes.

The efficiency of QSO selection in this work ($51/78 = 65$ per cent) is slightly larger than in FBQS-2 ($636/1130 =$

56 per cent). Although our selection criteria filter out most of the QSOs below $z = 3.5$, and these are covered by FBQS-2, our survey is better at rejecting galaxies, since we take the morphological information from SDSS whereas FBQS-2 used the less reliable APM discrimination. Although our sample has fewer sources, the efficiency for moderate to high redshift QSOs is high: $20/78 = 26$ per cent for $2 \leq z \leq 3.7$ compared to $65/1130 = 6$ per cent for FBQS-2. At $z \geq 3.7$ the efficiency of our selection is $10/78 = 13$ per cent. The maximum redshift in FBQS-2 is $z = 3.4$.

Table 4 compares the sizes and search efficiencies of various radio-selected high-redshift QSO samples. The success-rate for high- z QSOs and the number of QSOs in this work are comparable to or larger than those of previous searches for radio-selected QSOs at much *higher* radio flux densities.

4.4 The fraction of BAL QSOs

Twenty-six of the QSOs with spectra have redshifts $2.0 \leq z \leq 4.4$, so that Si IV 1397 Å and C IV 1549 Å are included in the observed wavelength range. Seven of these QSOs show strong broad absorption lines (BALs) with velocity widths above 2000 km s^{-1} and reaching velocities above 3000 km s^{-1} , and were classified as BALs. The balnicity index (BI) of each BAL was computed following the prescription of Weymann et al. (1991) and is presented in Table 5.

The fraction of BALs in our sample is therefore $7/26 = 27 \pm 10$ per cent. For comparison, from the study of the BAL QSOs in FBQS-2 (Becker et al. 2000) we derive an observed fraction of BALs for $1.5 \leq z \leq 3$ and $15 \leq E \leq 17.8$ of $14/134 = 10 \pm 3$ per cent (BALs with BI=0 excluded).

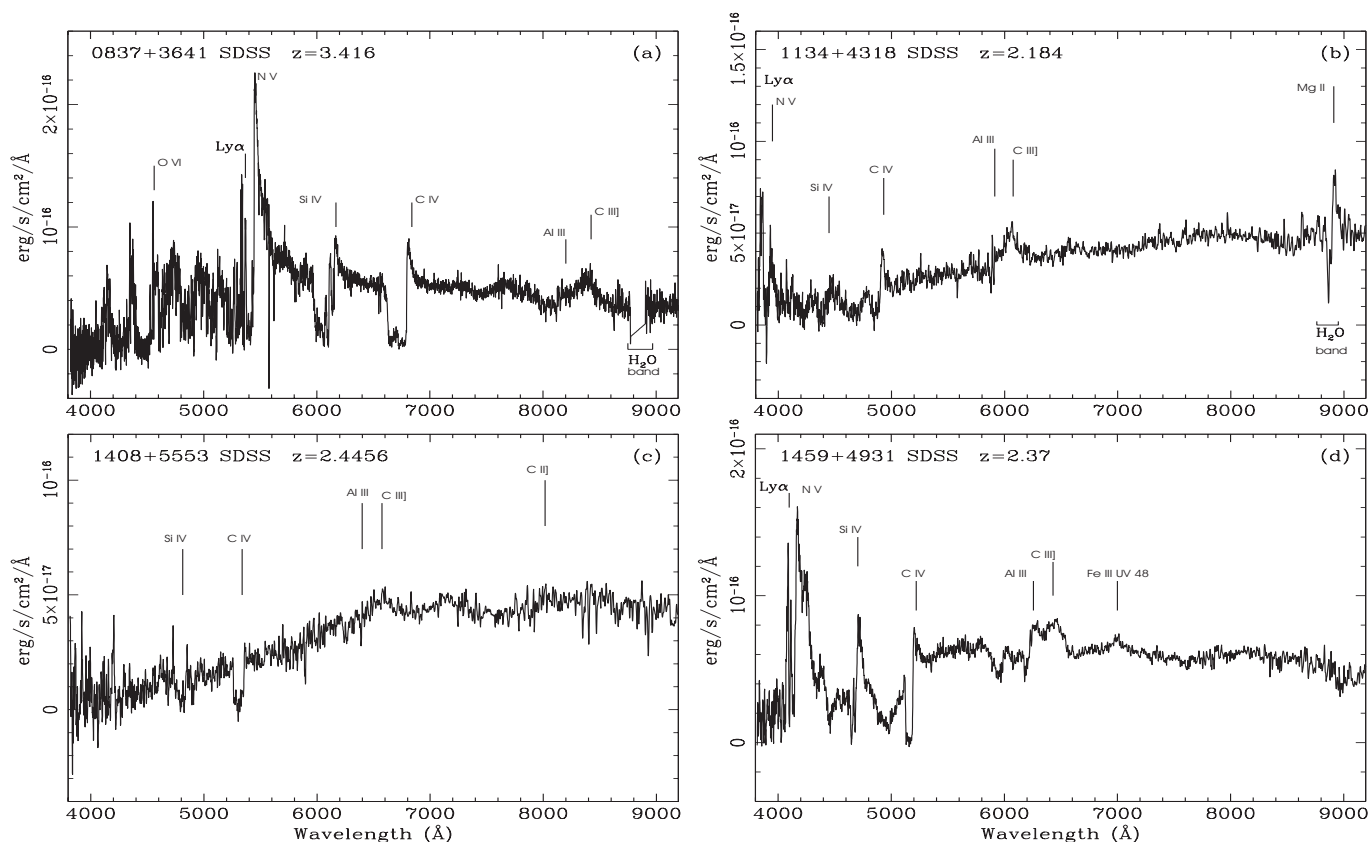


Figure 7. SDSS spectra of four of the seven $2 \leq z \leq 4.4$ BAL QSOs in the current sample. The three remaining spectra are presented in Fig. 1 of this paper, in Benn et al. (2002) and in Benn et al. (2005).

In view of the redder colours found for BALs, compared to non-BALs, and the adopted colour selection, $O - E \leq 2$, Becker et al. conclude that the BAL fractions derived from their work should be considered as lower limits. Our result, 27 ± 10 per cent, confirms a larger fraction of BALs in a red-selected sample ($O - E \geq 2$), and following their argument this value should be considered as an upper limit to the actual fraction. We note however, that the distribution of balnicity indices for the FBQS-2 BALs reaches lower values than the one in Table 5, which is more similar to the BI distribution of the BAL sample in Weyman et al. (1991), nowadays regarded as highly conservative. In particular we have 6/7 cases with $BI \geq 4500 \text{ km s}^{-1}$ (86 per cent), Weyman et al. 24/40 (60 per cent) and Becker et al. 6/14 (43 per cent). Because of our selection of the stronger BALs, in the comparison with FBQS-2 the fraction 27 ± 10 per cent should be regarded as a lower limit. Differences in the optical magnitudes and redshift ranges, along with small number statistics could explain the differences in the BAL fractions between FBQS-2, $> 10 \pm 3$ per cent, and our work, 27 ± 10 per cent.

Reichard et al. (2003a) obtained for a QSO sample selected from SDSS Early Data Release at $1.7 \leq z \leq 4.2$ (regardless of radio emission) an observed BAL fraction 14 ± 1 per cent. The BI distribution of these BALs reaches low values, with only $14/185 = 8$ per cent of them having $BI \geq 5000 \text{ km s}^{-1}$ (Reichard et al. 2003b). Reichard et al. (2003a) confirm that BAL QSOs are redder than non-BALs, and estimate a true BAL fraction of 13 ± 1 per cent, taking into

Table 5. Balnicity indices of the $z > 2$ BAL QSOs

FIRST name	z_{QSO}	BI km s^{-1}	BAL type	Spectrum
0837+3641	3.416	5600	LoBAL	SDSS, Fig. 7
1134+4318	2.184	9800	LoBAL?	SDSS, Fig. 7
1219+4849	3.201	4800	LoBAL	TNG, Fig. 1
1408+5553	2.446	4500		SDSS, Fig. 7
1459+4931	2.370	12850	LoBAL	SDSS, Fig. 7
1516+4309	2.59	6000	LoBAL	Benn et al. 2002
1624+3758	3.377	2990		Benn et al. 2005

account colour-dependent selection effects in BALs and non-BALs. Trump et al. (2006) found from a larger sample of SDSS DR3 QSOs at $1.7 \leq z \leq 4.38$ a slightly lower BAL fraction, 10.4 ± 0.2 per cent, with $BI \geq 5000 \text{ km s}^{-1}$ for $162/1756 = 9$ per cent of the BALs. For the comparison with our work and FBQS-2, the two last values should be regarded as upper limits, giving the low balnicity indices reached and the steeply rising distribution of BI towards low values (Reichard et al. 2003b). Taken together, the results from this work, Becker et al., Reichard et al. and Trump et al. suggest that the BAL fraction in radio-selected QSO samples is at least as high as that of optically-selected QSOs.

A brief description of the seven BALs is given below:

- FIRST 0837+3641 shows C IV and Si IV troughs starting at the QSO redshift, with a velocity width $\sim 8500 \text{ km}$

s^{-1} and sharp onset. The absorption bluewards of the expected Al III $\lambda 1860$ emission line suggests that this QSO is a low-ionization BAL (LoBAL).

- FIRST 1134+4318 shows C IV and Si IV troughs starting at the QSO redshift. The C IV absorption presents two clearly distinct components. The weak absorption bluewards of the expected Al III emission line suggests that this QSO could be a LoBAL.

- FIRST 1219+4849 shows C IV and Si IV troughs, the former starting sharply at the emission redshift and extending almost to the Si IV emission line. There is absorption bluewards of the Al III emission line, so this is probably a LoBAL, although some contamination by sky bands cannot be excluded.

- FIRST 1408+5553 shows C IV and Si IV troughs of width $\sim 5500 \text{ km s}^{-1}$, starting at the emission redshift.

- FIRST 1459+4931 shows C IV and Si IV troughs with a sharp onset at the emission redshift. The C IV absorption extends to the Si IV emission line and clearly shows two components. The strong Al III absorption confirms this QSO as a LoBAL. We identify the emission line at 7000 \AA as Fe III UV 48 (rest frame wavelengths 2062.2, 2068.9 and 2079.65 \AA , see Laor et al. 1997).

- FIRST 1516+4309, with deep C IV and Si IV troughs was firstly reported as a BAL in Benn et al. (2002). The absorption bluewards of the expected Al III suggests that this QSO is a LoBAL.

- FIRST 1624+3758 is an unusual BAL (Benn et al. 2005), with a clear detached C IV trough extending from -21000 to -29000 km s^{-1} .

The fraction of LoBALs in our sample, four to five out of seven or 55-70 per cent, is unusually high. For comparison, the observed fractions obtained from the FBQS-2 and from the SDSS BALs in Reichard et al. (2003a) are 28 ± 14 per cent (four out of fourteen) and 13 ± 3 per cent (24/181, $1.7 \leq z \leq 3.9$) respectively. The higher fraction in our sample is consistent with Becker et al. result that BALs in general and the LoBALs in particular are over-abundant among the reddest QSOs. Moreover, Reichard et al. (2003b) found that LoBALs have stronger CIV absorption troughs (i.e., stronger BI) than HiBALs, and the balnicity indices in our sample are in fact higher than the typical values in FBQS-2 and in Reichard et al.(2003a) SDSS sample.

4.5 The peculiar QSO FIRST 1413+4505

FIRST 1413+4505 (Fig. 2, $z = 3.107$) has an unusual spectrum, with a broad strong absorption starting at the expected position of the Ly α emission line and extending up to -18500 km s^{-1} bluewards. We identify the feature as H I on the basis of the location of the line and the detection of Ly β absorption at this redshift. The broad absorption is not detected in metal lines. The Ly α absorption feature has two components. The first one, at $z_{abs} = 3.06$, has a rest-frame EW $\sim 38 \text{ \AA}$ and associated Ly β absorption with EW $\sim 5 \text{ \AA}$. The second component, at $z_{abs} = 2.93$, has EW $\sim 7 \text{ \AA}$ and the corresponding Ly β absorption is difficult to identify due to the high noise in this part of the spectrum. The EW of the first Ly α absorber is consistent with a single damped Ly α system with high H I column density, i.e. $> 10^{21} \text{ cm}^{-2}$ (Lanzetta et al. 1991), at the QSO position. However, the

Ly α /Ly β ratio suggests an optically thin absorber, therefore the system could be a velocity-resolved BAL-like wind. A higher resolution spectrum is needed to determine the nature of this absorption system.

The spectral energy distribution of the source can be obtained from NED. The FIRST integrated flux density at 1.4 GHz is $140.3 \pm 0.1 \text{ mJy}$, and the flux density at 4.85 GHz is $125 \pm 15 \text{ mJy}$ (Becker, White & Edwards 1991). The source is unresolved in FIRST, < 1 arcsec. The SDSS magnitudes, corrected for Galactic extinction, are $u = 22.32 \pm 0.23$, $g = 20.15 \pm 0.04$, $r = 19.27 \pm 0.02$, $i = 19.09 \pm 0.02$ and $z = 19.09 \pm 0.05$. The source is not detected in 2MASS and the magnitude limits for 99% completeness are: $J = 15.8$, $H = 15.1$ and $K = 14.3$ (see 2MASS Web site[†]). FIRST 1413+4505 is highly luminous in the radio, $P_{1.4 \text{ GHz}} = 2.2 \times 10^{27} \text{ W Hz}^{-1}$, and has a flat radio spectral index, $\alpha = -0.09$. From the E magnitude and using the TNG spectrum for the k -correction we obtained $M_{AB}(1450 \text{ \AA}) = -25.7$ (see equations in Vigotti et al. 2003).

At the position of the QSO, mid-infrared emission is detected via 1D addition of IRAS Scans (SCANPI) at $12 \mu\text{m}$ and $25 \mu\text{m}$. The automatic procedure obtained via NED gives an 11σ detection at $12 \mu\text{m}$ in the addition modes ‘detector weighted’ and ‘mean’, 15σ detection for ‘rms weighted’ and non-detection for the ‘median’ mode. The corresponding peak flux densities in Jy are 0.22 ± 0.02 , 0.21 ± 0.02 and 0.31 ± 0.02 , respectively. At $25 \mu\text{m}$ coaddition gives 3.6σ detection for ‘detector weighted’ and ‘mean’ modes, 5σ for ‘rms weighted’ and non-detection with the ‘median’ mode. The corresponding peak flux densities are 0.08 ± 0.02 , 0.08 ± 0.02 and 0.11 ± 0.02 .

Mid-infrared detection at $z \geq 2$ is rare and we checked if the detection with SCANPI could arise due to confusion with one of the two bright stars 52 arcsec NE and 48 arcsec SW (binary) of the QSO, but neither of them was detected at $12 \mu\text{m}$ or $25 \mu\text{m}$.

Assuming that the mid-infrared emission is physically associated with the QSO, and not a chance coincidence, the luminosity of the QSO in the rest frame wavelength range $2200 \text{ \AA} - 6.1 \mu\text{m}$ (from z -band to $25 \mu\text{m}$ in the observer frame) would be $1.8 \times 10^{15} L_{\odot}$, i.e. FIRST 1413+4505 would be one of the most luminous objects known. To our knowledge there are five other systems with such extreme luminosities, and although they were discovered in different ways, and have different SEDs and absorption/emission-line properties, the extreme luminosity was in all cases ascribed to flux magnification due to gravitational lensing. These objects are the Seyfert 2 like object IRAS FSC 10214+4724 (Rowan-Robinson et al. 1991), the BAL QSO H1413+117 (Magain et al. 1988), the sub-mm galaxy SMM 02399-0136 (Iverson et al. 1998), the optically bright QSO APM 08279+5255 (Irwin et al. 1998) and the Lyman break galaxy MS 1512-cB58 (Yee et al. 1996).

4.6 The $z \geq 3.7$ QSO sample

Fig. 5 suggests that no QSOs with $z \geq 3.7$ will have been missed by the colour selection $O - E > 2$. The properties of the 10 $z > 3.7$ QSOs are given in Table 6. Adopting

[†] <http://www.ipac.caltech.edu/2mass>

Table 6. Absolute magnitudes, radio luminosities and contributions to space density, of the $z \geq 3.7$ QSOs

RA J2000 (1)	DEC J2000 (2)	z (3)	E (4)	$S_{1.4}$ mJy (5)	M_{AB} 1450 Å (6)	$\log P_{1.4}$ W Hz $^{-1}$ (7)	$z_{\min,o}$ (8)	$z_{\max,o}$ (9)	$z_{\max,r}$ (10)	z_a (11)	ρ Gpc $^{-3}$ (12)
09 41 19.44	51 19 33.0	3.850	18.02	2.49	-27.67	26.00	3.70	4.40	4.40	3.70-4.40	0.145
10 57 56.28	45 55 53.1	4.137	16.87	1.10	-28.37	25.70	3.70	4.40	4.38	3.70-4.38	0.149
11 02 01.91	53 39 12.7	4.297	19.64	4.45	-25.84	26.33					
11 10 55.22	43 05 10.1	3.862	18.08	1.21	-27.41	25.69	3.70	4.40	4.32	3.70-4.32	0.162
12 40 54.92	54 36 52.2	3.938	19.49	15.09	-25.85	26.80					
13 09 40.70	57 33 09.9	4.274	18.36	11.33	-26.59	26.73	3.85	4.40	4.40	3.85-4.40	0.187
15 06 43.81	53 31 34.4	3.790	17.89	14.63	-27.57	26.76	3.70	4.40	4.40	3.70-4.40	0.145
15 10 02.93	57 02 43.4	4.309	19.23	254.97	-26.53	28.09					
16 19 33.65	30 21 15.1	3.794	18.70	3.88	-26.96	26.18	3.70	4.40	4.40	3.70-4.40	0.145
16 39 50.52	43 40 03.7	3.990	17.68	25.23	-27.92	27.03	3.70	4.40	4.40	3.70-4.40	0.145

Cols. (1, 2, 3, 4, 5): similar to cols. (1, 2, 11, 6, 4) in Table 2. (6): absolute magnitude M_{AB} at rest-frame 1450 Å. (7): log radio luminosity at rest-frame 1.4 GHz. (8, 9, 10, 11): redshift limits in the optical ($z_{\min,o}$, $z_{\max,o}$), radio ($z_{\max,r}$), or both (z_a), within the range $3.7 \leq z \leq 4.4$. (12): contribution to the space density.

the magnitude limit $E \leq 19.1$, leaves 7 QSOs in the range $3.7 \leq z \leq 4.4$.

The absolute magnitudes at rest-frame 1450-Å, $M_{AB}(1450 \text{ Å})$, of the $z \geq 3.7$ QSOs were calculated from the extinction-corrected E magnitudes using the same procedure as in Vigotti et al. (2003), except for a better estimation of the k -corrections, obtained here from the individual spectra rather than using an average. We used the optical spectra from this work (FIRST 1110+4305), Benn et al. 2002 (FIRST 0941+5119) or from SDSS (remaining QSOs).

Fig. 8a shows $m_{AB}[1450(1+z)] - E$, or k -correction, for the redshift range 3.7 – 4.4, using the spectra of the 10 QSOs. Fig. 8b shows the mean and standard deviation of $m_{AB}[1450(1+z)] - E$ for the seven QSOs with $E \leq 19.1$.

The radio luminosities at rest-frame frequency of 1.4 GHz were calculated assuming a spectral index $\alpha = -0.3$ ($S_\nu \propto \nu^\alpha$), which is the median spectral index obtained for 13 $z > 3.6$ FIRST-APM QSOs in Holt et al. (2004). The radio luminosities range from $P_{1.4 \text{ GHz}} = 10^{25.7}$ to $10^{28.1}$ W Hz $^{-1}$, so all ten QSOs are ‘radio loud’ QSOs, adopting the criterion $P_{1.4 \text{ GHz}} > 10^{25.5}$ W Hz $^{-1}$ (Gregg et al. 1996).

4.6.1 Completeness of the $z \geq 3.7$, $E \leq 19.1$ QSO sub-sample

There are several sources of incompleteness, summarised below.

(1) Only 78 of the 94 candidates were spectroscopically classified, giving a fraction of 83 per cent.

(2) The APM completeness for $E \leq 19.1$ was estimated as the fraction of SDSS $r \leq 19.8$, $z \geq 2$ QSOs in the SDSS DR3 Quasar Catalog (Schneider et al. 2005) detected and starlike in APM E . The adopted r band limit was obtained from the average magnitude difference $r - E = 0.69$ (standard deviation 0.34) of the 10 high- z QSOs in the sample. Average $r - E$ and standard deviation for the 94 candidates are 0.55 and 0.36 respectively. From the 2060 DR3 QSOs in the surveyed area of this work, 2002 were detected in APM and 1793 of these were starlike, giving a fraction 87 ± 2 per cent.

(3) The completeness of the FIRST catalogue for the range 1 – 1.5 mJy is ~ 70 per cent (Prandoni et al. 2001).

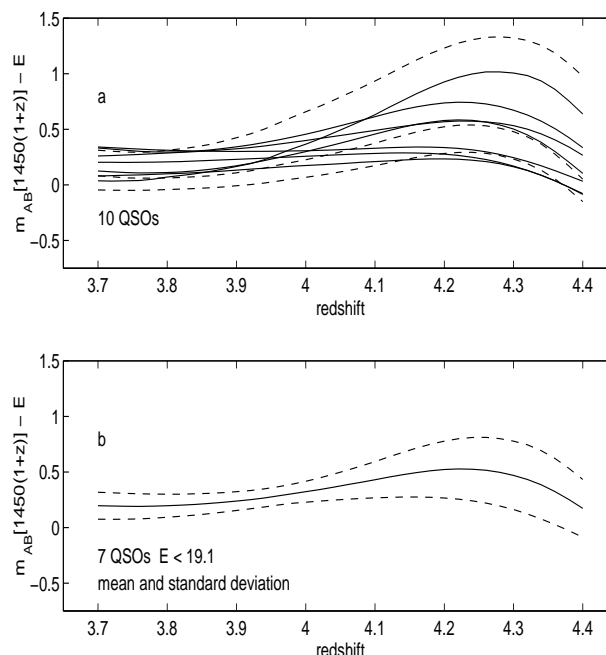


Figure 8. (a) k -correction between the AB magnitude at 1450 $(1+z)$ Å and through the E band, versus redshift, obtained from the spectra of the $z \geq 3.7$ QSOs. Solid lines correspond to the 7 QSOs with $E \leq 19.1$. (b) Average k -correction for these 7 QSOs (solid line) and standard deviation (dashed lines).

For the sample of seven QSOs, with radio flux densities: 1.1, 1.2, 2.5, 3.88, 11.33, 14.6 and 25.2 mJy, we estimate a completeness of 92 ± 5 per cent, assuming Poisson errors.

(4),(5) In Vigotti et al. (2003) we found for a very similar sample completeness 98 ± 1 per cent due to QSOs probably missed because of extended radio emission, and 99 per cent completeness due to QSOs that may exceed the radio-optical separation limit of 1.5 arcsec.

(6) From our work and from the literature (see Figs. 5, 6 and Section 4.2) we estimate 100 per cent completeness for the colour cut $O - E \geq 2$ in the redshift range 3.7 – 4.4.

(7) The completeness of the SDSS photometric survey quoted in the project web site, computed by comparing the

number of objects found by SDSS to the number found by the COMBO survey (Classifying Objects by Medium-Band Observations[§]), is 100 per cent for point sources with SDSS $r \leq 21$, which is above the maximum $r = 20.6$ in our sample.

The combined completeness due to the above seven factors is 64 ± 5 per cent.

5 QSO SPACE DENSITY AT HIGH-REDSHIFT

The observed space density of QSOs in the redshift range $3.7 \leq z \leq 4.4$, over the 1378.5 deg^2 survey area, was calculated using the sub-sample of seven QSOs with $E \leq 19.1$ and the $1/V_a$ estimator (see e.g. Avni & Bahcall 1980). The space density contributed by each QSO was computed as the inverse of the available volume, using the constraints $E \leq 19.1$, $S_{1.4 \text{ GHz}} \geq 1 \text{ mJy}$ and $3.7 \leq z \leq 4.4$. The redshift limits and the space density contribution of each QSO are listed in Table 6. The sum of these contributions yields a space density (for $M_{\text{AB}}(1450) \leq -26.6$) of $1.1 \pm 0.4 \text{ Gpc}^{-3}$, assuming Poisson errors. The mean redshift of the QSOs is 4.0, the mean absolute magnitude $M_{\text{AB}}(1450) = -27.5$ and the mean log radio luminosity $P_{1.4 \text{ GHz}} = 10^{26.3} \text{ W Hz}^{-1}$. Correcting for the 64 ± 5 per cent completeness, the space density is $1.7 \pm 0.6 \text{ Gpc}^{-3}$. Assuming the radio-loud fraction 13.4 ± 3 per cent for $P_{1.4 \text{ GHz}} \geq 10^{25.7} \text{ W Hz}^{-1}$ from Vigotti et al. (2003), the space density of all QSOs with $3.7 \leq z \leq 4.4$ and $M_{\text{AB}}(1450) \leq -26.6$ is $12.5 \pm 5.6 \text{ Gpc}^{-3}$.

5.1 Comparison with other surveys at $z \geq 3.7$

In Vigotti et al. (2003) we computed $\rho[M_{\text{AB}}(1450) \leq -26.9] = 7.4 \pm 2.6 \text{ Gpc}^{-3}$, at $3.85 \leq z \leq 4.45$, assuming the same radio-loud fraction as above. The average redshift (4.2), optical luminosity ($M_{\text{AB}}(1450) = -27.7$) and radio luminosity ($P_{1.4 \text{ GHz}} = 10^{26.6} \text{ W Hz}^{-1}$) were all slightly larger than for the current sample. Although the space density derived from the new sample has a larger statistical error, this work extends the computation of the space density to lower optical luminosities and benefits from better k -corrections.

Four of the seven $z \geq 3.7$ QSOs in the current work were also included in Vigotti et al. The $M_{\text{AB}}(1450)$ values obtained in the two analyses agree within 0.15 magnitudes, except for FIRST 1309+5733, with $M_{\text{AB}}(1450) = -26.6$ compared to -27.1 in Vigotti et al. The reason for the discrepancy is the high k -correction for this source (the highest among $E \leq 19.1$ QSOs in Fig. 8).

Fan et al. (2001a,b) obtained the space density of QSOs at high redshift using an SDSS-selected sample of 39 QSOs with $3.6 \leq z \leq 5.0$ and $-27.75 \leq M_{\text{AB}}(1450) \leq -25.5$. Seven of these QSOs have redshifts and absolute magnitudes within the range used here ($z = 3.7 - 4.4$, $M_{\text{AB}} \leq -26.6$) and in this sense our sample, with seven radio loud QSOs, has comparable quality in terms of the number of objects.

Fig. 9 shows the $1/V_a$ estimators of the cumulative luminosity function obtained in this work and in Vigotti et al., along with the maximum likelihood solution by Fan et al. For $z = 4.0$ Fan et al. give $\rho[M_{\text{AB}}(1450) \leq -26.6] = 8.0 \pm 4.6$

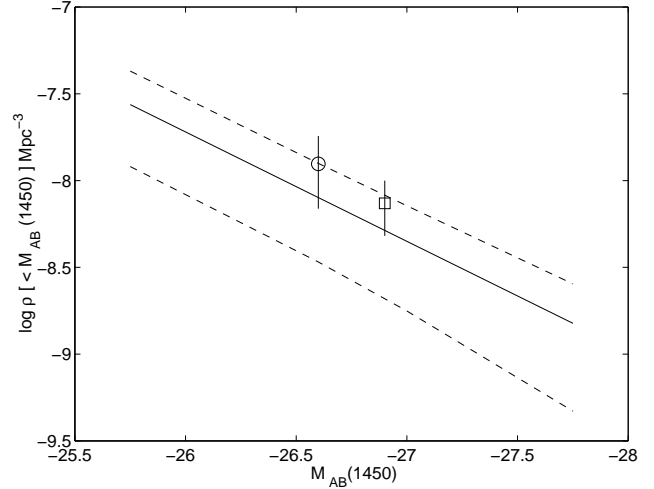


Figure 9. Cumulative luminosity function derived from the $1/V_a$ estimator in this work (circle, $3.7 \leq z \leq 4.4$) and in Vigotti et al. (square, $3.8 \leq z \leq 4.5$). Solid and dashed lines: maximum likelihood solution and standard deviation from Fan et al. ($3.6 \leq z \leq 5.0$).

Gpc^{-3} , compared to $12.5 \pm 5.6 \text{ Gpc}^{-3}$ in this work. These two values are consistent, within the errors.

6 CONCLUSIONS

A sample of 94 radio-emitting QSO candidates has been derived by cross-correlating the FIRST survey, APM POSS-I and the SDSS photometric survey, selecting objects with $E \leq 19.1$, $O - E \geq 2$, and starlike in SDSS. 78 of the 94 sources (83 per cent) are spectroscopically classified, mainly from SDSS, but also from the literature and from TNG spectroscopy presented here (13 sources). The classified sources include 51 QSOs, with redshifts $0.27 < z < 4.31$. Our main results are as follows:

(i) The efficiency of selection of high-redshift QSOs is $23/78 = 29$ per cent for $z \geq 3$, and $10/78 = 13$ per cent for $z \geq 3.7$, comparable to that for previous searches for high-redshift QSOs at much *higher* radio flux densities.

(ii) We found no $3.7 < z < 4.4$ QSOs with $2 < O - E < 3$, supporting our assumption that no $z > 3.7$ QSOs are missed by selecting $O - E \geq 2$.

(iii) The BAL fraction for the QSOs with $2 \leq z \leq 4.4$ in our sample is $\sim 27 \pm 10$ per cent ($7/26$), larger than found for FBQS-2 (Becker et al. 2000) and for the optically-selected SDSS samples in Reichard et al. (2003) and Trump et al. (2006), despite these three works being more complete for lower balnicity index. Our sample also has an unusually high fraction of LoBALs, four to five out of seven, compared to the above samples. The most likely explanation for the high frequency of BALs and LoBALs in our sample is the red colour selection, $O - E \geq 2$. A comparison of the three studies suggests that the BAL fraction in radio-selected QSO samples is at least as high as in optically-selected ones.

(iv) We note the unusual QSO FIRST 1413+4505 ($z = 3.11$), whose optical spectrum reveals a strong associated Ly α absorber (damped or BAL-like) that completely removes the Ly α emission. The source is highly luminous in

[§] <http://www.mpia-hd.mpg.de/COMBO>

the radio, has a flat radio spectral index, and is detected in *IRAS* 12 and 25 μm , yielding a bolometric luminosity in the range from SDSS z band to 25 μm $L \sim 1.8 \times 10^{15} L_{\odot}$, which places it amongst the most luminous objects known.

(v) Using a sub-sample of seven QSOs with $3.7 \leq z \leq 4.4$ and $E \leq 19.1$, we derive a space density of radio loud QSOs, $\rho[M_{\text{AB}}(1450) \leq -26.6, P_{1.4 \text{ GHz}} \geq 10^{25.7} (\text{W Hz}^{-1})] = 1.7 \pm 0.6 \text{ Gpc}^{-3}$. Assuming a radio-loud fraction 13.4 ± 3 per cent, the space density for all QSOs is $\rho[M_{\text{AB}}(1450) \leq -26.6] = 12.5 \pm 5.6 \text{ Gpc}^{-3}$. This result is in good agreement with the best-fitting model in Fan et al. (2001a,b), considering the statistical errors.

REFERENCES

- Abazajian K. et al. 2005, *AJ*, 129, 1755
 Avni Y., Bahcall J.N., 1980, *ApJ*, 235, 694
 Becker R.H., White R.L., Edwards A.L. 1991, *ApJS*, 75, 1
 Becker R.H., White R.L., Helfand D.J. 1995, *ApJ*, 450, 559
 Becker R.H., Gregg M.D., Hook I.M., McMahon R.G., White R.L., Helfand D.J. 1997, *ApJ*, 479, L93
 Becker R.H., White R.L., Gregg M.D., Brotherton M.S., Laurent-Muehleisen S.A., Arav N. 2000, *ApJ*, 538, 72
 Benn C.R., Vigotti M., Pedani M., Holt J., Mack K.-H. Curran R., Sánchez S.F. 2002, *MNRAS*, 329, 221 (Paper I)
 Benn C. R., Carballo R., Holt J., Vigotti M., González-Serrano J. I., Mack K.-H., Perley R. A. 2005, *MNRAS*, 360, 1455
 Evans D.W. 1989, *A&AS*, 78, 249
 Fan X. et al. 2001a, *AJ*, 121, 54
 Fan X. et al. 2001b, *AJ*, 121, 31
 Gregg M.D., Becker R.H., White R.L., Helfand D.J., McMahon R.G., Hook I.M. 1996, *AJ*, 112, 407
 Holt J., Benn C.R., Vigotti M., Pedani M., Carballo R., González-Serrano J.I., Mack K.-H., García B. 2004, *MNRAS*, 348, 857 (Paper II)
 Hook I.M., Becker R.H., McMahon R.G., White R.L. 1998, *MNRAS*, 297, 1115
 Hook I.M., McMahon R.G., Shaver P.A., Snellen I.A.G. 2002, *MNRAS*, 297, 1115
 Irwin M.J., Iбата R.A., Lewis G.F., Totten E.J. 1998, *ApJ*, 505, 529
 Ivezić Z. et al. 2002, *AJ*, 124, 2364
 Ivison R.J., Smail I., Le Borgne J.F., Blain A.W., Kneib J.P., BezzCourt J., Kerr T.H. 1998, *MNRAS*, 298, 583
 Kleinmann S.G. et al. 1994, *ApJS*, 217, 11
 Kopylov A. I., Artyukh V. S., Kopylova F. G. 2004, *A&A*, 421, 455
 Lanzetta K.M., Wolfe A.M., Turnshek L.L., McMahon R.G., Hazard C. 1991, *ApJS*, 77, 1
 Laor A., Jannuzi B.T., Green R.F., Boroson T.A. 1997, *ApJ*, 489, 656
 Magain P., Surdej J., Swings J.P., Borgeest U., Kayser R. 1988, *Nature*, 334, 325
 McMahon R.G., Irwin M.J. 1992, in MacGillivray H.T., Thomson E.B., eds, *Digitised Optical Sky Surveys*. Dordrecht:Kluwer, p. 417
 McMahon R.G., White R.L., Helfand D.J., Becker R.H. 2002, *ApJS*, 143, 1
 Najita J., Dey A., Brotherton M. 2000, *AJ*, 120, 2859
 Pennington R.L., Humphreys R.M., Odewahn S.D., Zumach W., Thurmes P.M. 1993, *PASP*, 105, 521
 Peroux C., Storrie-Lombardi L. J., McMahon R. G., Irwin M., Hook I. M. 2001, *AJ*, 121, 1799
 Prandroni I., Gregorini L., Parma P., de Ruiter H.R., Vettolani G., Wieringa M.H., Ekers R.D. 2001, *A&A*, 365, 392
 Reichard T.A. et al. 2003a, *AJ*, 126, 2594
 Reichard T.A. et al. 2003b, *AJ*, 125, 1711
 Rowan-Robinson M. et al. 1991, *Nature*, 351, 719
 Schlegel D.J., Finkbeiner D.P., Davis M. 1998, *ApJ*,
 Schneider D.P. et al, 2005, *AJ*, 130, 367
 Snellen I.A.G., McMahon R.G., Dennett-Thorpe J., Jackson N., Mack K.-H., Xanthopoulos E. 2001, *MNRAS*, 325, 1167
 Storrie-Lombardi L.J., McMahon R.G., Irwin M.J., Hazard C. 1996, *ApJ*, 468, 121
 Stoughton C. et al. 2002, *AJ*, 123, 485
 Vanden Berk D.E. et al. 2001, *AJ*, 122, 549
 Vigotti M., Carballo R., Benn C.R., de Zotti G., Fanti R., González-Serrano J.I., Mack K.-H., Holt J. 2003, *ApJ*, 591, 43
 Trump J.R. et al. 2006, *ApJS*, in press (astro-ph 0603070)
 Weymann R.J., Morris S.L., Foltz C.B., Hewett P.C. 1991, *ApJ*, 373, 23
 White R.L., Becker R.H., Helfand D.J., Gregg, M.D. 1997, *ApJ*, 475, 479
 White R.L. et al. 2000, *ApJS*, 126, 133
 Yee H.K. C., Ellington E., Bechtold J., Carlberg R.G. Cillandre J.C. 1996, *AJ*, 111, 1883

ACKNOWLEDGMENTS

We thank the referee for rapid and helpful feedback. RC, JIGS, CRB, and MV acknowledge financial support from the Spanish Ministerio de Educación y Ciencia under project AYA 2002-03326.

This research is in part based on observations made with the Italian Telescopio Nazionale Galileo (TNG) operated on the island of La Palma by the Fundación Galileo Galilei of the INAF (Istituto Nazionale di Astrofisica) at the Spanish Observatorio del Roque de los Muchachos of the Instituto de Astrofísica de Canarias. Funding for the creation and distribution of the SDSS Archive has been provided by the Alfred P. Sloan Foundation, the Participating Institutions, the National Aeronautics and Space Administration, the National Science Foundation, the U.S. Department of Energy, the Japanese Monbukagakusho, and the Max Planck Society. The SDSS Web site is <http://www.sdss.org/>. The SDSS is managed by the Astrophysical Research Consortium (ARC) for the Participating Institutions. The Participating Institutions are The University of Chicago, Fermilab, the Institute for Advanced Study, the Japan Participation Group, The Johns Hopkins University, the Korean Scientist Group, Los Alamos National Laboratory, the Max-Planck-Institute for Astronomy (MPIA), the Max-Planck-Institute for Astrophysics (MPA), New Mexico State University, University of Pittsburgh, University of Portsmouth, Princeton University, the United States Naval Observatory, and the University of Washington. This research has made use of the NASA/IPAC Extragalactic Database (NED) which is operated by the Jet Propulsion Laboratory, California Institute of Technology, under contract with the National Aeronautics and Space Administration. The 2MASS project is a collaboration between The University of Massachusetts and the Infrared Processing and Analysis Center (JPL/ Caltech). Funding is provided primarily by NASA and the NSF. The University of Massachusetts constructed and maintained the observatory facilities, and operated the survey.

Table 2. Radio/optical properties and spectroscopic classification of the 94 candidates

RA J2000 (1)	DEC J2000 (2)	FIRST-SDSS arcsec (3)	$S_{1.4}$ mJy (4)	$E(B - V)$ (5)	E (6)	$O - E$ (7)	SDSS (8)	Spectroscopic classification Other (9)	Class (10)	z (11)	Notes (12)
08 08 44.47	44 03 57.9	0.35	2.01	0.044	18.79	>3.18					
08 18 45.67	30 31 25.4	0.36	4.44	0.039	19.00	1.92	DR3		QSO	0.509	
08 20 50.19	42 19 01.9	0.68	4.34	0.054	15.42	2.40	DR3		late-type star		
08 37 49.60	36 41 45.5	0.14	27.10	0.039	18.65	2.75	DR3		QSO	3.416	
08 45 47.02	49 03 39.5	1.47	1.47	0.030	17.27	2.40	DR3		late-type star		
08 49 32.51	39 33 45.8	0.98	1.43	0.028	17.02	2.49	DR3		late-type star		
08 53 09.18	47 54 44.4	0.98	12.14	0.024	17.08	1.92		This work	late-type star		
08 53 37.88	42 54 28.1	1.37	1.92	0.030	18.95	>2.29	DR3		late-type star		
09 00 00.29	40 46 04.8	0.22	4.20	0.023	19.51	1.40	DR3		QSO	3.539	
09 16 52.79	39 27 14.7	0.48	2.73	0.013	18.25	1.93	DR3		QSO	0.269	a
09 40 03.02	51 16 02.7	0.16	13.91	0.011	18.47	2.11	DR3		QSO	3.601	
09 41 19.44	51 19 33.0	0.56	2.49	0.009	18.02	>3.69		Paper I	QSO	3.85	
09 43 10.67	42 30 16.7	0.49	1.79	0.012	19.02	2.03	DR3		QSO	0.737	
09 55 55.13	50 05 44.8	0.54	24.54	0.011	17.69	2.36					
09 56 55.77	52 57 11.7	0.85	1.47	0.011	18.40	3.10	DR3		late-type star		
10 07 48.74	54 12 52.1	1.25	1.07	0.008	18.26	3.07	DR3		late-type star		
10 08 02.07	42 18 39.3	0.24	1.42	0.017	19.35	1.69	DR3		QSO	1.872	
10 11 10.75	42 39 37.1	0.25	55.45	0.019	18.54	2.10	DR3	Literature	QSO	3.560	
10 34 01.84	50 07 46.5	0.20	3.35	0.014	17.09	2.41	DR3		early-type star		
10 39 02.18	49 31 39.1	0.30	1.50	0.012	19.48	1.79			QSO	1.09	b
10 39 15.68	47 05 41.1	0.73	395.44	0.015	19.51	1.63		Literature	QSO	2.36	c
10 46 57.16	48 27 23.8	0.11	37.54	0.015	18.62	2.01	DR3		QSO	1.287	
10 48 06.18	56 30 21.4	0.96	1.20	0.005	19.57	>2.30	DR3		QSO	1.905	
10 49 50.48	52 08 42.6	0.69	1.92	0.011	14.19	2.12					
10 57 56.28	45 55 53.1	0.44	1.10	0.012	16.87	3.77	DR4	Literature	QSO	4.137	
11 02 01.91	53 39 12.7	0.35	4.45	0.009	19.64	>2.09	DR3		QSO	4.297	
11 04 43.43	50 30 57.5	0.40	1.75	0.014	18.19	3.01					
11 10 55.22	43 05 10.1	0.39	1.21	0.014	18.08	3.66	DR4	This work	QSO	3.862	
11 24 36.15	47 02 20.5	0.30	3.38	0.020	18.72	2.82					
11 29 07.10	57 56 05.4	0.57	2.39	0.015	17.32	3.15	DR3		ELG	0.312	d
11 29 56.16	51 33 46.5	0.40	3.21	0.013	18.94	1.98	DR3		QSO	2.955	
11 30 43.08	51 41 33.9	0.68	4.01	0.015	17.66	3.12	DR3	Paper I	late-type star		
11 32 56.63	43 54 27.7	1.25	1.29	0.023	19.58	>1.97					
11 34 45.83	43 18 58.0	0.14	28.00	0.023	18.69	2.14	DR4		QSO	2.184	
11 35 51.30	42 45 18.1	0.20	1.82	0.026	19.41	1.97	DR4		QSO	0.387	
11 36 27.96	56 43 41.8	0.63	123.34	0.015	18.68	2.39	DR4		QSO	0.88	

Table 2. Continued

RA J2000 (1)	DEC J2000 (2)	FIRST-SDSS arcsec (3)	$S_{1,4}$ mJy (4)	$E(B - V)$ (5)	E (6)	$O - E$ (7)	SDSS (8)	Other (9)	Spectroscopic classification Class (10)	z (11)	Notes (12)
11 37 27.31	47 33 41.5	0.82	1.34	0.022	19.84	>2.22					
11 40 34.95	44 23 38.9	0.09	3.47	0.025	18.10	2.30					
11 47 49.80	49 28 07.0	0.26	68.81	0.016	19.82	2.31					
11 53 13.06	56 51 26.3	0.39	27.86	0.017	19.06	2.49	DR3		QSO	1.201	
12 10 21.46	46 36 01.9	1.40	1.05	0.015	19.91	>2.38					
12 19 57.18	48 49 27.0	0.41	6.92	0.015	19.69	>2.86		This work	QSO	3.201	
12 20 42.41	48 09 06.9	0.42	2.06	0.014	17.82	3.21	DR3		late-type star		
12 27 03.19	50 53 56.3	0.20	3.87	0.016	18.49	2.32	DR3		QSO	0.765	
12 31 38.14	57 53 42.8	0.88	1.96	0.012	16.42	2.89	DR3		late-type star		d
12 34 27.25	45 19 55.6	0.37	2.07	0.012	20.18	2.06	DR4	This work	QSO	3.466	
12 40 54.92	54 36 52.2	0.14	15.09	0.023	19.74	>1.85	DR3		QSO	3.938	
12 47 10.29	55 55 57.4	1.20	10.25	0.012	19.58	1.57	DR3		QSO	0.498	
13 08 01.18	53 07 51.3	0.19	8.89	0.016	18.08	2.70	DR3		QSO	0.322	
13 09 40.70	57 33 09.9	0.08	11.33	0.016	19.49	>3.35	DR3	Paper I	QSO	4.274	
13 10 03.35	53 53 48.3	0.11	14.45	0.020	19.34	2.11	DR3		QSO	3.278	
13 13 30.11	51 46 41.4	0.64	1.60	0.013	18.96	3.32					
13 19 43.44	44 03 50.2	0.03	1.13	0.015	20.22	>1.90					
13 23 30.44	54 59 55.6	0.21	5.22	0.022	18.76	3.22	DR3		QSO	2.208	e
13 29 28.23	50 54 34.1	1.23	2.95	0.011	18.52	2.74					
13 34 01.81	55 27 33.0	0.40	1.51	0.010	18.13	2.86	DR3		late-type star		
13 42 36.96	43 26 32.1	0.09	26.87	0.013	19.06	2.35	DR3		QSO	1.044	
13 43 11.80	43 05 34.8	0.02	53.21	0.013	20.59	2.11		This work	QSO	0.897	
13 53 06.01	55 08 35.2	0.87	1.91	0.009	19.41	2.04	DR3		early-type star		
13 58 29.83	42 39 55.3	1.18	1.52	0.008	15.60	2.64		This work	late-type star		
14 01 22.22	44 01 57.2	0.68	1.02	0.009	19.43	1.96	DR4		QSO	1.238	
14 05 51.56	51 55 17.9	0.22	1.34	0.017	19.45	2.17		This work	ELG	0.2705	
14 08 15.25	55 53 46.5	0.23	3.41	0.015	19.29	>3.08	DR3		QSO	2.446	
14 13 18.87	45 05 23.0	0.11	140.31	0.007	19.27	1.67	DR4	This work	QSO	3.107	f
14 20 13.66	50 48 55.6	0.55	2.69	0.018	19.64	>2.31					
14 20 33.71	57 39 01.0	0.12	4.28	0.011	18.58	2.72	DR3		QSO	0.736	d
14 22 43.02	44 17 21.5	0.09	1.25	0.008	18.14	2.59	DR4	This work	QSO	3.564	
14 31 41.08	51 56 42.5	0.33	1.49	0.011	19.67	2.16					
14 36 06.62	47 25 32.0	0.07	207.70	0.022	18.73	2.35		This work	QSO	0.943	
14 40 10.73	50 55 56.0	0.71	2.05	0.013	19.75	>2.42	DR3		late-type star		
14 55 25.95	48 57 01.6	0.25	8.25	0.022	19.39	1.86	DR3		QSO	3.492	
14 59 26.33	49 31 36.9	0.09	5.22	0.019	18.71	1.69	DR3		QSO	2.370	

Table 2. Continued

RA J2000 (1)	DEC J2000 (2)	FIRST-SDSS arcsec (3)	$S_{1.4}$ mJy (4)	$E(B - V)$ (5)	E (6)	$O - E$ (7)	SDSS (8)	Spectroscopic classification		z (11)	Notes (12)
								Other (9)	Class (10)		
15 02 26.89	48 37 11.5	0.29	34.26	0.020	18.24	1.97	DR3	Literature	QSO	3.209	
15 02 59.54	45 12 55.1	0.52	5.21	0.023	18.43	2.31		This work	late-type star		
15 06 43.81	53 31 34.4	0.46	14.63	0.015	17.89	3.06	DR3		QSO	3.79	
15 09 39.01	43 46 48.8	0.53	1.02	0.015	18.47	>3.20	DR4		late-type star		e
15 10 02.93	57 02 43.4	0.34	254.97	0.012	19.23	>2.04	DR3	Literature	QSO	4.309	
15 16 01.52	43 09 31.5	0.63	1.34	0.027	18.50	>3.11	DR3	Paper I	QSO	2.59	e
15 39 38.48	55 10 33.4	1.38	4.20	0.014	19.15	>2.91	DR3		late-type star		
15 46 17.71	40 00 35.6	1.03	2.41	0.015	18.38	2.63	DR4		late-type star		e
15 48 43.10	39 14 58.4	1.25	2.59	0.010	18.45	2.91	DR4		late-type star		e
15 50 59.05	37 07 22.5	0.43	6.07	0.021	17.40	2.14	DR4		QSO	0.588	e,g
15 56 33.78	35 17 57.4	0.29	31.72	0.023	19.07	2.14	DR4	Literature	QSO	1.501	e
16 06 28.19	32 27 10.7	0.64	25.99	0.032	17.85	2.82	DR4		late-type star		e
16 10 07.07	39 41 32.8	0.44	1.13	0.009	18.61	2.37	DR3		late-type star		
16 11 50.68	43 44 12.8	0.24	1.20	0.012	17.97	3.02	DR3		late-type star		
16 17 23.13	32 28 18.3	0.27	1.43	0.022	17.97	2.57					g
16 19 33.65	30 21 15.1	0.36	3.88	0.028	18.70	>3.18	DR4		QSO	3.794	e
16 21 11.28	37 46 04.9	0.17	643.09	0.013	18.85	2.38	DR3		QSO	1.273	
16 24 53.48	37 58 06.6	0.10	56.44	0.011	18.47	2.03	DR3	Paper II	QSO	3.377	
16 33 17.71	42 51 08.4	0.14	1.45	0.008	19.18	1.65		This work	QSO	3.130	
16 35 35.35	35 24 17.2	0.43	5.18	0.026	18.50	2.76	DR3	Paper I	late-type star		
16 36 34.46	31 58 54.2	1.16	1.63	0.023	16.80	2.40		This work	late-type star		
16 39 50.52	43 40 03.7	0.37	25.23	0.012	17.68	3.55	DR3	Paper I	QSO	3.99	

Cols. (1,2): SDSS coordinates. (3): radio-optical (FIRST-SDSS) separation. (4): FIRST 1.4 GHz flux density (integrated for $S_{1.4 \text{ GHz}} > 10$ mJy, otherwise peak, see fig. 4 in Ivezić et al. 2002). (5): $E(B - V)$ Galactic extinction (Schlegel, Finkbeiner & Davis 1998). (6,7): E magnitude and $O - E$ colour taken from McMahon et al. (2002) FIRST-optical identification catalogue (APM magnitudes recalibrated with respect to APS, for more accurate photometry), and corrected for Galactic reddening assuming $A(E) = 2.7E(B - V)$ and $A(O) = 4.4E(B - V)$ (see White et al. 2000); (8,9,10,11): source of spectrum, spectroscopic classification, and redshift. The references from the literature are as follows: FIRST 1011+4239 and FIRST 1502+4837, Snellen et al. 2001; FIRST 1039+4705, Kopylov, Artyukh & Kopylova 2004; FIRST 1057+4555, Peroux et al. 2001; FIRST 1510+5702, Storrie-Lombardi et al. 1996; and FIRST 1556+3517, Najita, Dey & Brotherton 2000. (12): Notes as follows: a = Not a QSO in the “DR3 Quasar Catalog”, probably because it doesn’t meet the requirement $M_i > -22$ ($H_0 = 70 \text{ km s}^{-1} \text{ Mpc}^{-1}$, $\Omega_M = 0.3$, and $\Omega_\Lambda = 0.7$), b = Classified in this work from the presence of CIII] and MgII emission lines in the SDSS DR3 spectrum, c = Spectrum not published, d = The source is not included in McMahon et al. (2002), therefore the APM calibration was adopted, e = spectrum not available on the SDSS website, f = See Section 4.5, g = Classified as a galaxy in 2MASS (The Two Micron All Sky Survey, Kleinmann et al. 1994)